

# Unexpected stability of $[\text{Cu}\cdot\text{Ar}]^{2+}$ , $[\text{Ag}\cdot\text{Ar}]^{2+}$ , $[\text{Au}\cdot\text{Ar}]^{2+}$ , and their larger clusters

N. R. Walker, R. R. Wright, P. E. Barran, H. Cox, and A. J. Stace

*School of Chemistry, Physics, and Environmental Science, University of Sussex, Falmer, Brighton BN1 9QJ, United Kingdom*

(Received 21 November 2000; accepted 9 January 2001)

Experimental observations following the ionization of neutral group 11 metal/argon complexes have revealed the presence of doubly charged ions of the form  $[\text{M}\cdot\text{Ar}_n]^{2+}$  for  $n$  in the range 1–6. Of particular interest are two features of the results. First, the unexpected stability of the dimer ions,  $[\text{M}\cdot\text{Ar}]^{2+}$ , since similar species involving a molecule rather than a rare gas atom are often unstable with respect to charge transfer. *Ab initio* calculations show the dimers owe their stability to a combination of a strong electrostatic interaction and the high ionization energy of argon. A second feature to the results is the high relative intensities of the  $[\text{M}\cdot\text{Ar}_4]^{2+}$  and  $[\text{M}\cdot\text{Ar}_6]^{2+}$  ions. Calculations show these complexes to consist of square-planar  $D_{4h}$  structures, with the additional two atoms in  $[\text{M}\cdot\text{Ar}_6]^{2+}$  occupying axial sites, which are Jahn–Teller distorted. The calculated relative binding energies support the preferential stability of these two structures. © 2001 American Institute of Physics. [DOI: 10.1063/1.1352036]

## I. INTRODUCTION

The criteria established for the appearance of a doubly charged atomic or molecular cluster depend upon a subtle balance between repulsive and attractive forces.<sup>1,2</sup> A doubly charged cluster could be viewed as “thermodynamically” stable if all routes to decay are endothermic; in contrast, “kinetic” stability implies a metastable state, from which there exists at least one exothermic reaction channel. Homonuclear dimer and trimer ions,  $\text{A}_{2,3}^{2+}$ , invariably fall into the latter category, where a strong Coulomb repulsion is counteracted by the formation of a weakly-bound state,<sup>1</sup> which in some instances correlates with excited-state atomic ions.<sup>3</sup> For the more general case of a heteronuclear system,  $\text{AX}_{1,2}^{2+}$ , the reasons for formation of a bound state can be summarized as either (i) a curve crossing between a repulsive  $\text{A}^+ + \text{X}_{1,2}^+$  potential surface and a bound  $\text{A}^{2+} + \text{X}_{1,2}$  state. The dominant contributions to the latter being ion-induced dipole and (for a molecule) ion–dipole interactions, or (ii) a combination of covalent bonding plus Coulomb repulsion.<sup>1,2</sup> Echt and Märk have identified a third class of small doubly charged cluster,<sup>1</sup> and this corresponds to the situation where all the charge is located on a single atom or molecule, e.g.,  $\text{A}^{2+}\cdot\text{X}_{1,2}$ . Thermodynamic stability is achieved when the ionization energy of X is larger than the second ionization energy of A. Several mixed rare gas dimer ions have been found to fall within this category,<sup>1,4</sup> as has a series of rare gas–molecule clusters.<sup>5</sup> Although some slight energy mismatch may be accommodated through contributions from solvation energy, doubly charged complexes involving rare gases are normally considered to be very susceptible to charge transfer followed by Coulomb-induced fragmentation. Fewer examples of metastability have been identified for small systems, although  $\text{NeKr}^{2+}$ ,<sup>6</sup>  $\text{Mg}^{2+}\cdot\text{H}$ , and  $\text{HCl}^{2+}$  would appear to fall into the latter category.<sup>7</sup> Gill and Radom have analyzed data on a range of doubly charged cations in

terms of a simple model that equates stability with the position of a surface crossing which defines charge transfer.<sup>7</sup>

Reported here are the results of a series of experiments and calculations undertaken on complexes of the form  $[\text{M}\cdot\text{Ar}_n]^{2+}$  where M is either copper, silver, or gold and  $n$  ranges from 1–8. Given the large differences between the second ionization energies (IE) of these metals ( $\text{M}^+ \rightarrow \text{M}^{2+}$  values are given in Table I) and the IE of an argon atom (15.75 eV), charge transfer might have been expected. In cases where the M(II) state of either of these metals is associated with a polyatomic,<sup>8–12</sup> such as pyridine, it has been observed that two or more molecules are frequently required to form a stable complex. However, for argon, reproducible ion signals have been recorded for  $[\text{Cu}\cdot\text{Ar}]^{2+}$  and  $[\text{Ag}\cdot\text{Ar}]^{2+}$ , and calculations show that  $[\text{Au}\cdot\text{Ar}]^{2+}$  should also be stable. There is experimental evidence of larger  $[\text{M}\cdot\text{Ar}_n]^{2+}$  clusters for all three metals. Metal–rare gas doubly charged ions of the form  $[\text{Mg}\cdot\text{Ar}_n]^{2+}$  have been observed previously by Velegrakis and Luder, and found to exhibit an intensity maximum at  $n=6$ .<sup>13</sup> However, unlike the group 11 metals,  $[\text{Mg}\cdot\text{Ar}_n]^{2+}$  clusters are kinetically stable in that the second IE of Mg at 15.07 eV is lower than that of an argon atom. Fanourgakis and Farantos have interpreted the  $[\text{Mg}\cdot\text{Ar}_n]^{2+}$  results using a combination of *ab initio* calculation and electrostatic interactions, and they found that  $[\text{Mg}\cdot\text{Ar}_6]^{2+}$  corresponds to a regular octahedron.<sup>14</sup> Other examples taken from experimental studies of doubly charged metal ion–molecule interactions have provided numerous instances of charge transfer, and semiquantitative models have proved to be very successful at interpreting these data.<sup>15,16</sup> In contrast, most *ab initio* theoretical investigations have been limited to doubly charged complexes that are kinetically stable.<sup>17,18</sup>

TABLE I. Ionization energies (IE) of copper, silver, and gold.<sup>a</sup>

	Copper	Silver	Gold
1st IE/eV	7.73	7.58	9.22
2nd IE/eV	20.29	21.5	20.5

<sup>a</sup>Ionization energy of argon: 15.75 eV.

## II. EXPERIMENTAL SECTION

A detailed description of the general instrumentation used for generation, resolution, and detection of the cluster beam has been provided in previous work.<sup>11</sup> Briefly, argon carrier gas at a pressure of between 30 and 40 psi, undergoes supersonic expansion through a 200  $\mu\text{m}$  diameter conical nozzle, followed by collimation 2 cm downstream by a 1 mm diameter skimmer. Midway between the expansion chamber and the mass spectrometer, the cluster beam passes over the mouth of a high temperature effusion cell (DCA Instruments, EC-40-63-21) equipped with a crucible of pyrolytic boron nitride, in which metal vapor is generated. In order to maximize the surface area of metal, the cell is positioned at a slight angle ( $\cong 30^\circ$ ) with respect to the vertical. Metal vapor is allowed to diffuse into the flight tube in order to create a region where the vapor and the cluster beam can interact. Metal atom attachment occurs via a pickup process that involves the evaporation of rare gas atoms to stabilize the neutral complex.<sup>11</sup>

Signal intensities measured on the apparatus over a series of experiments have suggested that the optimal partial pressure of metal vapor is between  $10^{-1}$  and  $10^{-2}$  torr. Above this pressure, disruption of the cluster beam results in reduced signal intensity, and at lower pressures the metal/argon cluster signals decrease. For copper, the above partial pressure was estimated from the observation that the effusion cell operated most effectively when the temperature was held at 1350  $^\circ\text{C}$ , as measured with a standard C-type thermocouple. For silver and gold the optimum temperatures were 1100  $^\circ\text{C}$  and 1500  $^\circ\text{C}$ , respectively. Formation of neutral metal/argon clusters results from the collision of metal atoms with argon clusters, with kinetic energy from the collision and the solvation energy of the neutral metal atom being dispersed by the ejection of argon atoms. Del Mistro and Stace have presented a theoretical description of the pickup process.<sup>19</sup>

A shutter at the exit of the effusion cell is used to confirm the identity of clusters containing metal ions. Where a survey has been performed of the relative intensities of parent ions of a given series, the difference was taken between the signal intensity with the shutter open and closed. This approach removes any contribution from background signal that is not dependent on material originating from the effusion cell. Confirmation of the distribution of relative intensities for  $[\text{Cu}\cdot\text{Ar}_n]^{2+}$  and  $[\text{Ag}\cdot\text{Ar}_n]^{2+}$  clusters can be found by utilizing both metal isotopes.

The neutral metal/argon clusters were ionized by 100 eV electrons within the ion source of a high resolution, double focusing mass spectrometer (VG ZAB-E), and were then accelerated by a potential of +5 kV. After passing through a field-free region, ions were selected according to their mass/

charge ratio in a magnetic sector. When referenced to the mass increment separating singly charged ions, doubly charged species appeared in the mass spectra at half-integer intervals. A second field-free region separates the magnetic sector from an electrostatic analyzer (ESA), and the presence of a gas cell in this region permits the collisional activation of size-selected parent ions. For selected complexes their fragmentation processes have been examined in the presence of  $\sim 10^{-6}$  mbar of air as a collision gas. The fragments arising from CID were identified by scanning the ESA in the form of MIKE (mass-analyzed ion kinetic energy) scans.<sup>20</sup> These scans were performed on doubly charged ions with kinetic energies of 10 keV, which allowed for straightforward detection and verification of fragment ions resulting from Coulomb explosion. Final ion detection took place at a Daly detector, where phase sensitive detection was facilitated by a Stanford Research Systems SR850 lock-in amplifier.

## III. COMPUTATIONAL DETAILS

All geometry optimizations were performed using the MP4(SDQ) method (Møller–Plesset perturbation theory truncated at fourth-order, including all single, double, and quadruple substitutions) and the LANL2DZ basis set. LANL2DZ is a double-zeta basis set which, for post-third row atoms, includes some relativistic effects due to the effective core potential representations of electrons near the nuclei. Calculation of the  $[\text{M}\cdot\text{Ar}]^{2+}$  potential energy curves utilized full MP4, including triple substitutions, with an augmented LANL2DZ basis set. All calculations were performed using GAUSSIAN98.<sup>21</sup> For the  $\text{M}^{2+} + \text{Ar}$  curves an initial guess wave function at each metal–argon distance was calculated. To obtain the  $\text{M}^+ + \text{Ar}^+$  curve a single point energy was calculated at large  $R$ , which for Cu and Ag produced a point on the  $\text{M}^{2+} + \text{Ar}$  curve. Therefore, in order to produce the lower energy dissociation limit,  $\text{M}^+ + \text{Ar}^+$ , the argon highest occupied molecular orbital (HOMO) was swapped with a metal  $d$ -orbital from the valence set [usually the lowest unoccupied (LUMO) or SLUMO]. This new wave function was then scanned backwards to yield an estimate of

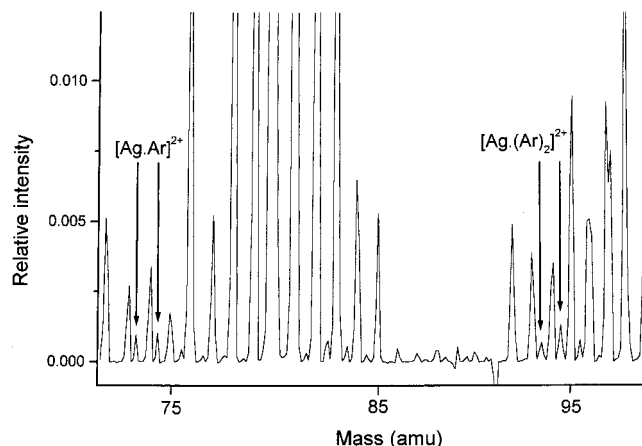


FIG. 1. Section of a mass spectrum showing the presence of  $[\text{Ag}\cdot\text{Ar}]^{2+}$  and  $[\text{Ag}\cdot(\text{Ar})_2]^{2+}$ . Confirmation that these ions contain silver comes from using the shutter on the Knudsen cell. The mass spectrum is dominated by singly charged by-products of the pickup technique used to prepare complexes.

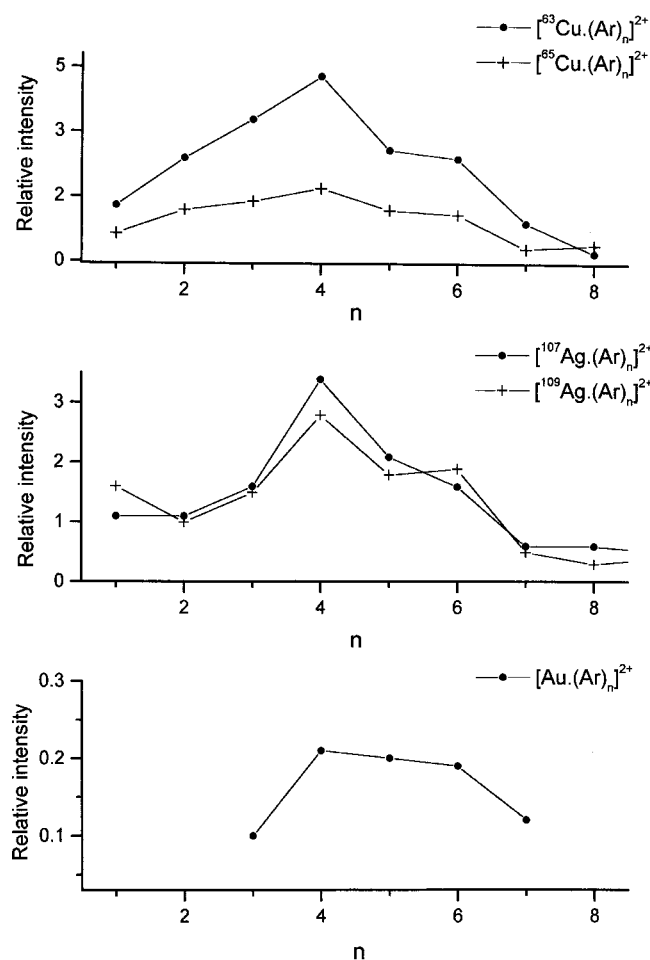


FIG. 2. Relative intensity distributions for the ions  $[\text{Cu}\cdot\text{Ar}_n]^{2+}$ ,  $[\text{Ag}\cdot\text{Ar}_n]^{2+}$ , and  $[\text{Au}\cdot\text{Ar}_n]^{2+}$  plotted as a function of  $n$ . Where appropriate measurements have been made using both metal isotopes, where for  $^{63}\text{Cu}$ : $^{65}\text{Cu}$  the intensity ratio is approximately 3:1, and for  $^{107}\text{Ag}$ : $^{109}\text{Ag}$  the ratio is approximately 1:1.

the avoided crossing position. The same procedure was applied to  $[\text{Au}\cdot\text{Ar}]^{2+}$ , but in this case it was not necessary to switch orbitals.

#### IV. RESULTS AND DISCUSSION

Figure 1 shows a short section of a mass spectrum recorded following the ionization of mixed silver/argon clusters. In addition to the cluster ions of interest, the preparative technique leads to a wide range of singly and doubly charged by-products. Included in this latter group are pure argon cluster ions with various isotopic combinations, and argon clusters containing traces of water,  $\text{O}_2$ , and  $\text{N}_2$  and their fragmentation products. Figure 2 gives the relative intensities of  $[\text{Cu}\cdot\text{Ar}_n]^{2+}$ ,  $[\text{Ag}\cdot\text{Ar}_n]^{2+}$ , and  $[\text{Au}\cdot\text{Ar}_n]^{2+}$  cluster ions plotted as a function of  $n$ . Since the overall intensities of the  $[\text{Au}\cdot\text{Ar}_n]^{2+}$  ions were much lower than those of clusters containing the other two metals, it proved difficult to undertake accurate measurements when  $n \leq 2$ . For copper and silver the trend in intensity as a function of  $n$  is reproduced by measurements on both isotopes. As a function of size, the three metals exhibit identical behavior: each distribution increases to a peak at  $[\text{M}\cdot\text{Ar}_4]^{2+}$  and then drops slightly for

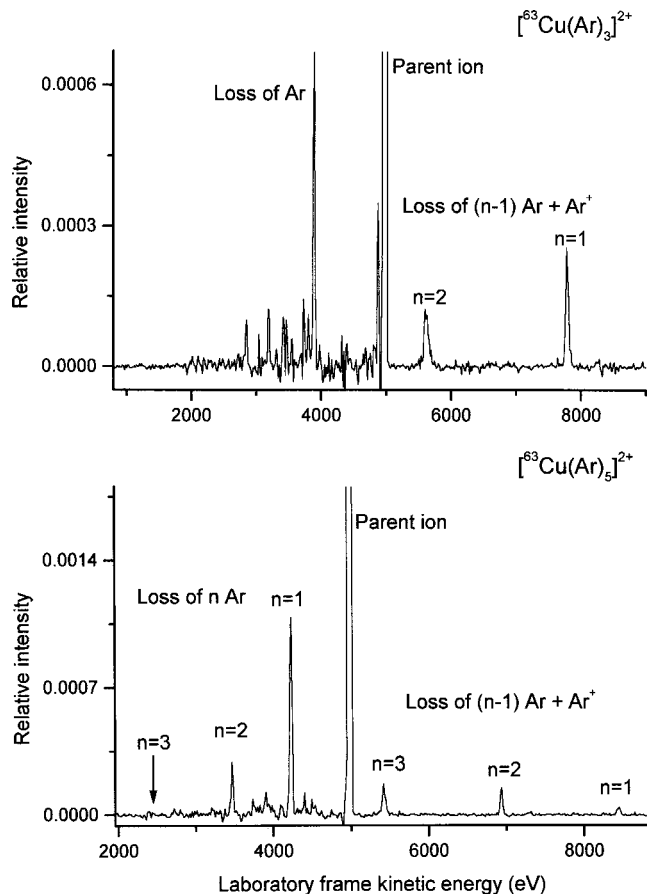


FIG. 3. MIKE scans recorded for  $[\text{Cu}\cdot\text{Ar}_3]^{2+}$  and  $[\text{Cu}\cdot\text{Ar}_5]^{2+}$ . The relative intensities of fragment ions are plotted as a function of their laboratory-frame kinetic energies.

$[\text{M}\cdot\text{Ar}_5]^{2+}$  and  $[\text{M}\cdot\text{Ar}_6]^{2+}$  before undergoing a sharp decline beyond  $n=6$ . Several groups have previously noted comparatively intense signals corresponding to the stable singly charged combinations  $\text{M}^+\cdot\text{Ar}_4$  and  $\text{M}^+\cdot\text{Ar}_6$ ,<sup>22–26</sup> but both are not always seen for the same metal. However, the pattern of behavior shown in Fig. 2 for the region  $n=3–7$ , is remarkably similar to that recorded by Velegrakis *et al.* for  $\text{Ni}^+\text{Ar}_n$  and  $\text{Pt}^+\text{Ar}_n$  clusters.<sup>26</sup> We shall return to a discussion of these points later in the text.

Figure 3 shows the results of two experiments undertaken on the collision-induced fragmentation of size-selected  $[\text{Cu}\cdot\text{Ar}_n]^{2+}$  complexes for  $n=3$  and 5. In each case, the parent ion is transmitted through the electrostatic analyzer at a laboratory-frame kinetic energy of 5 keV. Products arising from the unimolecular loss of neutral atoms are to be seen at kinetic energies lower than 5 keV, while products resulting from unimolecular loss accompanied by charge transfer can be seen anywhere in the kinetic energy range 0–10 keV. For the smaller of the complexes, there is a significant charge transfer product, with the loss of  $\text{Ar}^+$  dominating this route. The efficiency of this particular step has been noted in other experiments on Cu(II) complexes,<sup>10</sup> and is believed to be driven by the underlying stability of the  $\text{Cu}^+\cdot\text{L}_2$  unit, which in the condensed phase is linear.<sup>27</sup> For  $[\text{Cu}\cdot\text{Ar}_5]^{2+}$  the dominant fragmentation pathway is the loss of a single, neutral argon atom, which would equate with the observation in the

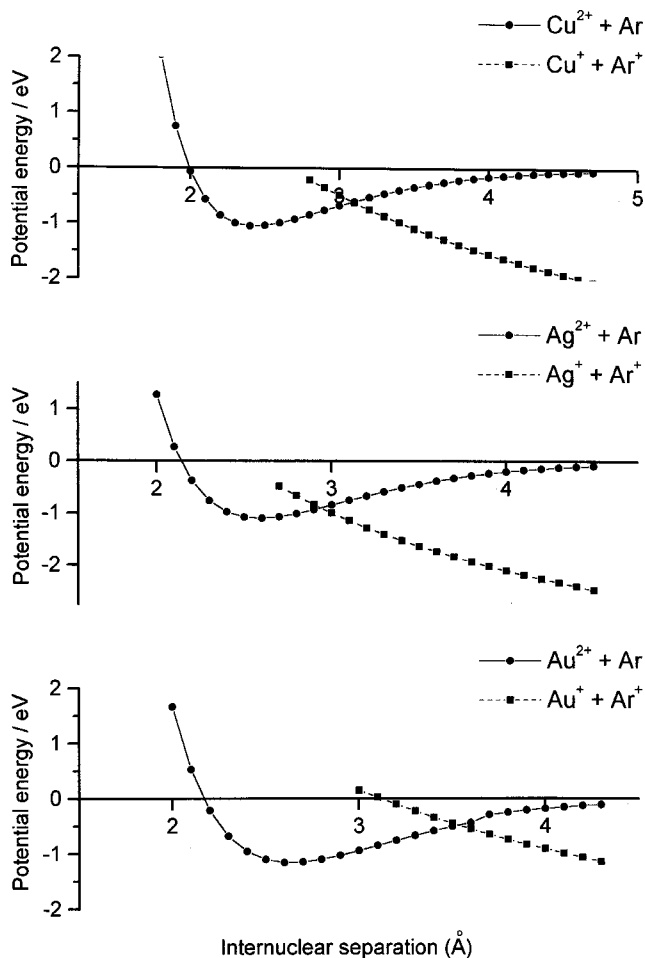


FIG. 4. Calculated potential energy curves for the  $[\text{M}\cdot\text{Ar}]^{2+}$  dimer ions plotted as a function of internuclear separation. Details of the well depths and locations of the avoided crossings are given in Table II.

mass spectrum of a comparatively intense signal for  $[\text{Cu}\cdot\text{Ar}_4]^{2+}$ . As the complexes increase in size the probability of collision-induced charge transfer diminishes in favor of neutral atom loss. The widths of the charge transfer peaks shown in Fig. 3, reflect the kinetic energy released as a result of Coulomb repulsion between the two separating positive charges. The peak widths recorded for the  $[\text{M}\cdot\text{Ar}_n]^{2+}$  complexes are very narrow in comparison to those seen for other  $[\text{M}\cdot\text{L}_n]^{2+}$  systems, where L is a polyatomic ligand.<sup>8–11</sup> This difference can be attributed directly to the much higher ionization energy of argon compared with that of a typical polyatomic ligand, for example, pyridine at 9.25 eV.

### A. The stability of $[\text{M}\cdot\text{Ar}]^{2+}$ ions

The first aspect of the results that needs to be examined is the reason for the stability of the  $[\text{M}\cdot\text{Ar}]^{2+}$  dimer ions. Figure 4 shows potential energy curves calculated for interactions between the pairs  $\text{M}^{2+} + \text{Ar}$ , and  $\text{M}^+ + \text{Ar}^+$ . As expected, the latter interaction is purely repulsive; however, the ion-neutral potential curve contains a stable well, which together with the location of the (avoided) surface crossing appears to provide sufficient conditions for the appearance of stable ions. In all three cases the well depth is  $\sim 1$  eV; however, with regard to observing a stable diatom, the important

TABLE II. Locations of the avoided crossings and the binding energies of  $[\text{M}\cdot\text{Ar}]^{2+}$  dimer ions.

$[\text{M}\cdot\text{Ar}]^{2+}$	Binding energy/eV <sup>a</sup>	Avoided crossing/Å
$[\text{Cu}\cdot\text{Ar}]^{2+}$	0.439	3.09
$[\text{Ag}\cdot\text{Ar}]^{2+}$	0.199	2.94
$[\text{Au}\cdot\text{Ar}]^{2+}$	0.670	3.35

<sup>a</sup>Defined as the well depth minus the potential energy at the surface crossing.

quantity is the well depth lying below the crossing point. These values together with the positions of the avoided crossings are listed in Table II. The principal intermolecular interaction responsible for each potential well, can be identified from the fact that the combination of a Coulomb repulsive potential and an attractive ion-induced dipole interaction, gives curve crossings that are within  $\pm 0.1$  Å of those given in Table II. Thus, the reduced surface crossing distance seen for  $[\text{Ag}\cdot\text{Ar}]^{2+}$  in comparison to the other two metals, can be attributed directly to the higher second ionization energy of silver. Overall the three doubly charged dimers owe their stability to a combination of high ionization energy and moderate polarizability on the part of the argon atom. Although comparatively small, the binding energy calculated for  $[\text{Ag}\cdot\text{Ar}]^{2+}$  is certainly sufficient to accommodate one or more bound states. Since the route leading to the observation of bound dimers probably involves argon evaporation, cooling associated with the latter process will help to stabilize the resultant ions. For  $[\text{Au}\cdot\text{Ar}]^{2+}$  the calculated binding energy is the highest of the three systems studied; however, we believe experimental factors to be responsible for our failure to observe this ion.

### B. Preferential stability of $[\text{M}\cdot\text{Ar}_4]^{2+}$ and $[\text{M}\cdot\text{Ar}_6]^{2+}$ ions

Having accounted for the stability of the basic dimer building-block, the addition of further argon atoms to form the larger doubly charged units should proceed without destabilizing the clusters. Thus, subsequent calculations have concentrated on explaining the relative stability of the  $[\text{M}\cdot\text{Ar}_4]^{2+}$  ion, and the effects of adding one and two further argon atoms; however, for the sake of completeness, all structures containing between two and six argon atoms have been investigated. All three doubly charged metal ions have electronic configurations corresponding to  $[\text{Rg}]nd^9$ , where  $n = 3, 4,$  or  $5$  for  $\text{Cu}^{2+}$ ,  $\text{Ag}^{2+}$ , or  $\text{Au}^{2+}$ , respectively. Based on current knowledge of more traditional  $\text{Cu}^{2+}$  complexes,<sup>27</sup> together with the limited data available on those of  $\text{Ag}(\text{II})$ ,<sup>28,29</sup> the structure anticipated for all three  $[\text{M}\cdot\text{Ar}_4]^{2+}$  clusters should be square-planar, with the  $d_{x^2-y^2}$  orbital holding the single electron. Such behavior is confirmed by the calculations, and sample structures for all  $[\text{M}\cdot\text{Ar}_n]^{2+}$  complexes for  $n$  in the range 2–6 are shown in Fig. 5. Since all three metals yielded structures that are qualitatively similar only one set, that of  $[\text{Cu}\cdot\text{Ar}_n]^{2+}$ , is shown in Fig. 5; however, details of internuclear separation and charge distribution for the individual metal ions are summarized in Table III. All the  $[\text{M}\cdot\text{Ar}_4]^{2+}$  complexes are calculated to be

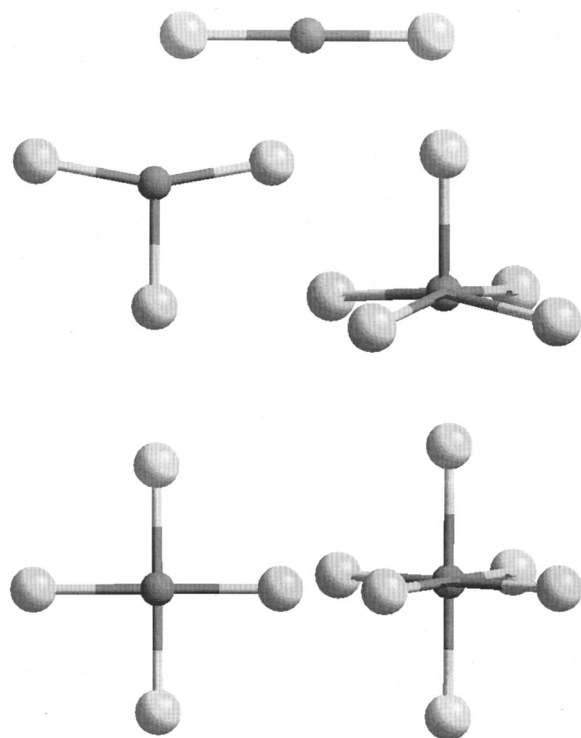


FIG. 5. Calculated structures for  $[\text{Cu}\cdot\text{Ar}_n]^{2+}$  complexes with  $n$  in the range 2–6. Structures involving the other two metal cations are very similar to these. Details of bond lengths and angles are given in Table III.

square-planar and have a  ${}^2B_{1g}$  electronic ground state. These structures are identical to those calculated by Velegarakis *et al.* for  $\text{Ni}^+\cdot\text{Ar}_4$  and  $\text{Pt}^+\cdot\text{Ar}_4$ ,<sup>26</sup> which is not too unex-

TABLE III. Calculated properties of  $[\text{M}\cdot\text{Ar}_n]^{2+}$  complexes for  $\text{M}$ =copper, silver, or gold.

Complex	Structure	Inter atomic separation		Charge distribution		
		$[\text{M}-\text{Ar}]^{\text{a}}/\text{\AA}$	$[\text{M}-\text{Ar}]^{\text{b}}/\text{\AA}$	$\text{M}/q^{\text{c}}$	$\text{Ar}^{\text{a}}/q^{\text{c}}$	$\text{Ar}^{\text{b}}/q^{\text{c}}$
$[\text{CuAr}]^{2+}$	$C_{\infty v}$	2.4298		1.75	0.25	
$[\text{AgAr}]^{2+}$		2.5873		1.72	0.28	
$[\text{AuAr}]^{2+}$		2.6362		1.69	0.31	
$[\text{CuAr}_2]^{2+}$	$D_{\infty h}$	2.4294		1.52	0.24	
$[\text{AgAr}_2]^{2+}$		2.6139		1.51	0.25	
$[\text{AuAr}_2]^{2+}$		2.6517		1.44	0.28	
$[\text{CuAr}_3]^{2+}$	$C_{2v}$	2.4795	2.5203	1.36	0.22	0.20
$[\text{AgAr}_3]^{2+}$		2.6390	2.6930	1.35	0.23	0.19
$[\text{AuAr}_3]^{2+}$		2.6786	2.7215	1.26	0.26	0.23
$[\text{CuAr}_4]^{2+}$	$D_{4h}$	2.5428		1.23	0.19	
$[\text{AgAr}_4]^{2+}$		2.6817		1.20	0.20	
$[\text{AuAr}_4]^{2+}$		2.7176		1.08	0.23	
$[\text{CuAr}_5]^{2+}$	$C_{4v}$	2.5717	2.6830	1.12	0.18	0.15
$[\text{AgAr}_5]^{2+}$		2.6970	2.9521	1.13	0.19	0.11
$[\text{AuAr}_5]^{2+}$		2.7383	2.9776	1.01	0.22	0.13
$[\text{CuAr}_6]^{2+}$	$D_{4h}$	2.5957	2.7542	1.03	0.17	0.13
$[\text{AgAr}_6]^{2+}$		2.7117	2.9836	1.07	0.18	0.10
$[\text{AuAr}_6]^{2+}$		2.7606	2.9992	0.94	0.20	0.12

<sup>a</sup>Equatorial argon atoms.

<sup>b</sup>Axial argon atoms.

<sup>c</sup> $q$ , the charge is in units of an electron.

TABLE IV. Average and incremental binding energies for  $[\text{M}\cdot\text{Ar}_n]^{2+}$  complexes, where  $\text{M}$  is copper, silver, or gold. The units are electron volts and the values given do not include zero-point energy.

$n$	$[\text{Cu}\cdot\text{Ar}_n]^{2+}$		$[\text{Ag}\cdot\text{Ar}_n]^{2+}$		$[\text{Au}\cdot\text{Ar}_n]^{2+}$	
	Av. BE <sup>a</sup>	Inc. BE <sup>b</sup>	Av. BE <sup>a</sup>	Inc. BE <sup>b</sup>	Av. BE <sup>a</sup>	Inc. BE <sup>b</sup>
1	1.154		1.101		1.145	
2	1.045	0.936	0.966	0.831	1.051	0.958
3	0.899	0.606	0.824	0.538	0.909	0.623
4	0.812	0.552	0.760	0.569	0.843	0.644
5	0.728	0.390	0.661	0.267	0.733	0.294
6	0.661	0.329	0.593	0.252	0.656	0.272

<sup>a</sup>Average binding energy as defined by Eq. (1).

<sup>b</sup>Incremental binding energy as defined by Eq. (2).

pected since  $\text{Ni}(\text{I})$  and  $\text{Pt}(\text{I})$  are isoelectronic with  $\text{Cu}(\text{II})$  and  $\text{Au}(\text{II})$ , respectively. Where differences do exist between the singly and doubly charged complexes, is in the degree of charge delocalization away from the metal. As Table III shows, a significant fraction of the total charge has moved from  $\text{Au}(\text{II})$  onto the argon atoms.

The addition of two further argon atoms to any of the  $[\text{M}\cdot\text{Ar}_4]^{2+}$  complexes, will involve filling the vacant axial positions where they will encounter a filled  $d_z^2$  orbital. As a result, the axial atoms will be partially shielded from the charge on the metal core, and although the calculations show that these additional atoms are still bound to the complexes via the central metal ion, their internuclear separations and binding energies reflect the reduced level of interaction with  $\text{M}^{2+}$ . Each of the calculated  $[\text{M}\cdot\text{Ar}_6]^{2+}$  structures appears to be a classic example of Jahn–Teller distortion in a near perfect system, i.e., the full effect of orbital degeneracy ( $d^9$  in  $O_h$  symmetry) is experienced by ligands which are themselves unperturbed by interactions with nearest-neighbors. As can be seen from Table III, the difference in internuclear separation between equatorial and axial atoms for octahedral complexes is between 0.2 and 0.27  $\text{\AA}$ , which is quite significant. Likewise, atoms occupying the separate sites are distinguished by carrying markedly different fractions of the delocalized positive charge. Again these distorted  $O_h$  structures ( $D_{4h}$  square bipyramids) are similar to those identified by Velegarakis *et al.* for  $\text{Ni}^+\cdot\text{Ar}_6$  and  $\text{Pt}^+\cdot\text{Ar}_6$ .<sup>26</sup> The results presented here regarding Jahn–Teller distortion in  $[\text{Ag}\cdot\text{Ar}_6]^{2+}$  follow a similar trend to those presented by Akesson *et al.*<sup>30</sup> in an *ab initio* study of  $[\text{Ag}\cdot(\text{H}_2\text{O})_6]^{2+}$ . The data for gold are certainly the first example of Jahn–Teller distortion in a  $\text{Au}(\text{II})$  complex.

Table IV lists the average binding energies, which were calculated on the basis of a reaction energy corresponding to the step



Similarly, incremental binding energies were calculated according to a reaction energy for the process



and these are also given in Table IV and plotted for all three metals in Fig. 6. In each case it can be seen that between  $[\text{M}\cdot\text{Ar}_3]^{2+}$  and  $[\text{M}\cdot\text{Ar}_6]^{2+}$  there are plateaus of stability,

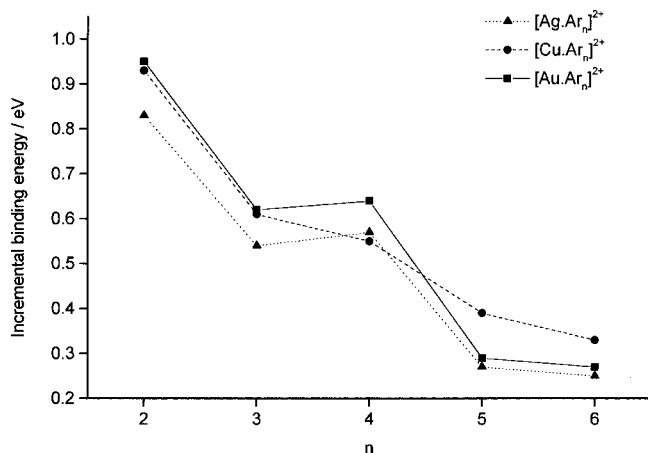


FIG. 6. Calculated incremental binding energies of the  $[\text{M}\cdot\text{Ar}_n]^{2+}$  complexes plotted as a function of  $n$ . These data were calculated according to Eq. (2) and the numerical values are given in Table IV.

which are particularly pronounced for silver and gold. For ions of the latter two metals, the results suggest that their complexes actually gain slightly in stability on going from  $[\text{M}\cdot\text{Ar}_3]^{2+}$  to  $[\text{M}\cdot\text{Ar}_4]^{2+}$ ; for  $[\text{M}\cdot\text{Ar}_5]^{2+}$  and  $[\text{M}\cdot\text{Ar}_6]^{2+}$ , the results show the complexes to have comparable binding energies. Support for the preferential stability of Au(II)/rare gas square-planar complexes is to be found in very recent observations by Seidel and Seppelt.<sup>31</sup> These authors have succeeded in preparing and characterizing a crystalline compound containing square-planar  $[\text{Au}\cdot\text{Xe}_4]^{2+}$ .

### C. The structures of $[\text{M}\cdot\text{Ar}_n]^{2+}$ for $n=2, 3$ , and 5

Starting with the  $[\text{M}\cdot\text{Ar}_2]^{2+}$  complexes, all of which are seen to be linear, the structures of larger clusters were identified by adding single atoms and reoptimizing the geometries. All three  $[\text{M}\cdot\text{Ar}_3]^{2+}$  structures were calculated to be nearly T-shaped, with  $[\text{Cu}\cdot\text{Ar}_3]^{2+}$  exhibiting the largest degree of distortion. The factors responsible for such behavior are similar to those present in the interhalogen compounds, e.g.,  $\text{ClF}_3$ ,<sup>27</sup> where structure is influenced by repulsive interactions between filled orbitals. The starting structure for  $[\text{M}\cdot\text{Ar}_5]^{2+}$  was formed by adding a fifth Ar atom to the square-planar base derived for  $[\text{M}\cdot\text{Ar}_4]^{2+}$ . However, it was found that all the calculations converged to an arrangement consisting of the fifth atom weakly bound to a *distorted* square-planar base as shown in Fig. 5. Again the structures are not unlike those found for the interhalides, e.g.,  $\text{IF}_5$ .<sup>27</sup>

It is interesting to note that the calculated binding energies of the  $[\text{Ag}\cdot\text{Ar}_n]^{2+}$  complexes are all consistently lower than those of either  $[\text{Cu}\cdot\text{Ar}_n]^{2+}$  or  $[\text{Au}\cdot\text{Ar}_n]^{2+}$ . It would appear that the destabilizing influence of the reduced surface crossing distance seen for  $[\text{Ag}\cdot\text{Ar}]^{2+}$  also extends to the larger cluster ions. Similar behavior in more realistic systems, e.g.,  $[\text{Ag}\cdot(\text{pyridine})_n]^{2+}$  could have important implications for the stability of transition metal complexes.<sup>32</sup> However, this factor does not appear to extend to the structures of the clusters or their internuclear separations, which follow an order suggested by their ionic radii, i.e.,  $\text{Cu}^{2+} < \text{Ag}^{2+} < \text{Au}^{2+}$ .

## V. CONCLUSION

Observations on the appearance and relative intensities of  $[\text{M}\cdot\text{Ar}_n]^{2+}$  ions for  $\text{M}=\text{copper, silver, and gold}$ , have been interpreted successfully using *ab initio* methods. Stability of the dimer ions,  $[\text{M}\cdot\text{Ar}]^{2+}$ , with respect to charge transfer is attributed to a combination of polarizability and high ionization energy on the part of argon. Comparatively intense complexes consisting of the combinations  $[\text{M}\cdot\text{Ar}_4]^{2+}$  and  $[\text{M}\cdot\text{Ar}_6]^{2+}$  are found to have  $D_{4h}$  structures, with the latter having additional atoms occupying axial positions, which are Jahn–Teller distorted. All three metals exhibit a very similar pattern of behavior.

## ACKNOWLEDGMENTS

H.C. and A.J.S. would like to thank Professor J. N. Murrell and Dr. T Wright for helpful discussions, and H.C. would like to thank EPSRC for the award of an Advanced Research Fellowship. All calculations were performed on an ONYX 2 belonging to the Sussex High Performance Computing Initiative.

- O. Echt and T. D. Märk, in *Clusters of Atoms and Molecules II*, edited by H. Haberland (Springer-Verlag, Berlin, 1994), p. 183.
- S. D. Price, *J. Chem. Soc., Faraday Trans.* **93**, 2451 (1997).
- M. Barysz and P. Pyykkö, *Chem. Phys. Lett.* **325**, 225 (2000).
- H. Helm, K. Stephan, T. D. Mark, and D. L. Huestis, *J. Chem. Phys.* **74**, 3844 (1981).
- N. G. Gotts and A. J. Stace, *Int. J. Mass Spectrom. Ion Processes* **102**, 151 (1990).
- K. Stephan, T. D. Mark, and H. Helm, *Phys. Rev. A* **26**, 2981 (1982).
- P. M. W. Gill and L. Radom, *Chem. Phys. Lett.* **136**, 294 (1987).
- A. J. Stace, N. R. Walker, and S. Firth, *J. Am. Chem. Soc.* **119**, 10239 (1997).
- N. R. Walker, S. Firth, and A. J. Stace, *Chem. Phys. Lett.* **292**, 125 (1998).
- R. R. Wright, N. R. Walker, S. Firth, and A. J. Stace, *J. Phys. Chem.* (to be published).
- N. R. Walker, R. R. Wright, and A. J. Stace, *J. Am. Chem. Soc.* **121**, 4837 (1999).
- N. R. Walker, R. R. Wright, P. E. Barran, and A. J. Stace, *Organometallics* **18**, 3569 (1999).
- M. Velegrakis and C. Luder, *Chem. Phys. Lett.* **223**, 139 (1994).
- G. S. Fanourgakis and S. C. Farantos, *J. Phys. Chem.* **100**, 3900 (1996).
- R. Tonkyn and J. C. Weisshaar, *J. Am. Chem. Soc.* **108**, 7128 (1986).
- J. C. Weisshaar, *Acc. Chem. Res.* **26**, 213 (1993).
- S. Petrie and L. Radom, *Int. J. Mass. Spectrom.* **192**, 173 (1999).
- K. N. Kirschner, *J. Chem. Phys.* **112**, 10228 (2000).
- G. Del Mistro and A. J. Stace, *Chem. Phys. Lett.* **196**, 67 (1992).
- R. G. Cooks, J. H. Beynon, R. M. Caprioli, and G. R. Lester, *Metastable Ions* (Elsevier, Amsterdam, 1973).
- GAUSSIAN98, Revision A.7, M. J. Frisch, G. W. Trucks, H. B. Schlegel *et al.*, Gaussian, Inc., Pittsburgh, PA, 1998.
- R. G. Cooks, J. H. Beynon, R. M. Caprioli, and G. R. Lester, *Metastable Ions* (Elsevier, Amsterdam, 1973).
- D. E. Lessen and P. J. Brucat, *Chem. Phys. Lett.* **149**, 10 (1988).
- D. E. Lessen and P. J. Brucat, *J. Chem. Phys.* **91**, 4522 (1989).
- M. Beyer, C. Berg, G. Albert, U. Achatz, and V. E. Bondybey, *Chem. Phys. Lett.* **280**, 459 (1997).
- M. Velegrakis, G. E. Froudakis, and S. C. Farantos, *J. Chem. Phys.* **109**, 4687 (1998).
- F. A. Cotton and G. W. Wilkinson, *Advanced Inorganic Chemistry* (Wiley, London, 1988).
- W. Levanson and M. D. Spicer, *Coord. Chem. Rev.* **76**, 45 (1987).
- H. N. Po, *Coord. Chem. Rev.* **20**, 171 (1976).
- R. Akesson, L. G. M. Pettersson, M. Sandström, and U. Wahlgren, *J. Am. Chem. Soc.* **116**, 8691 (1994).
- S. Seidel and K. Seppelt, *Science* **290**, 117 (2000).
- N. R. Walker, R. R. Wright, P. E. Barran, J. N. Murrell, and A. J. Stace (unpublished).